Mechanics & Industry **21**, 614 (2020)
© AFM, EDP Sciences 2020
https://doi.org/10.1051/meca/2020086

Mechanics & Industry

Available online at:
www.mechanics-industry.org

Regular Article

Shape effects on aerodynamic loading of heliostats

Hakim Merarda[1,2,*], Mounir Aksas[3], and Thomas Andrianne[4]

[1] Department of Mechanics, Faculty of Technology, University of Batna 2, Batna, Algeria
[2] Unité de Recherche Appliquée en Énergies Renouvelables, Centre de Développement des Énergies Renouvelables, Ghardaïa, Algeria
[3] Energetics Applied Physics Laboratory, University of Batna 1, Batna, Algeria
[4] Department of Aerospace and Mechanical Engineering, University of Liège, Liège, Belgium

Received: 11 June 2020 / Accepted: 28 October 2020

Abstract. The effect of the shape of the mirror of a heliostat is studied through wind tunnel tests in uniform smooth and turbulent flow conditions. Three shapes are investigated: square (reference case), octagonal and circular geometries. The forces and moments are measured on reduced scale models of heliostats in low, medium and strong turbulence wind conditions in a uniform wind profile. The turbulence intensity of the flow is adjusted in the wind tunnel test section by the adjunction of passive grids upstream the model. The experimental results are presented for several elevation and azimuth angles. The results showed that: in smooth flow conditions, the geometry of the mirror has very limited effect on the mean force coefficient, while impacting the fluctuating part of the aerodynamic loads. In turbulence flow conditions, the circular mirror/panel is advantageous for the aerodynamic design of the elevation drive and mirror support structure.

Keywords: Heliostat / mirror shape / aerodynamic load / wind tunnel / solar tower plant

1 Introduction

Heliostats are generally equipped with two-degree-of-freedom tracking systems following the sun during the day. In the case of Solar Power Tower Plant (SPTP), the tower receives concentrated sunlight reflected by the mirrors placed on the heliostats. This thermal energy collected on the receiver is used later in a classical thermodynamic energy production cycle. One of the key challenges in the SPTP is the cost reduction of field of heliostats [1]. The optimal design and selection of suitable parts, including the foundation, driving mechanism, structural support and reflecting surface, as well as the fitted dimensions allow a significant cost reduction in heliostats erection [2]. The cost of materials for structural components in larger heliostats is most sensitive to the predicted wind speed [3].

The wind loads are found to be sensitive to both the geometric scale and frequency content of the flow [4]. In this work, Emes et al. studied the dependence of the peak wind load coefficients on a heliostat in stow position on turbulence characteristics in the atmospheric boundary layer. Their results show that the lift and hinge moment coefficients increase linearly with increasing of the turbulence intensity and the ratio of integral length scale to mirror chord length increase with increasing the Reynolds number.

The literature on wind effects on heliostats is rich in techniques to reduce as much as possible the aerodynamic forces. Peterka et al. [5] carried out simulations of flow over heliostats at a 1:60 scale in operational positions in the plant. They showed that wind loads can be reduced to values below of those acting on isolated unit by using a perimeter wind fences. They also pointed out that wind loads decrease as the position of the heliostat is close to the receiving tower (combination of heliostat angles and position).

Pfahl and Uhlemann [6] studied the Reynolds number effects on wind loads applied on solar trackers at stow position. They concluded that a Reynolds number effect is not important for this position. Meanwhile, Pfahl et al. [7] studied the wind load coefficients on single heliostats of aspect ratios between 0.5 and 3.0. The method consists in investigating solar trackers with mirrors of 30 m2 at a reduced scale of 1:20. They concluded that higher aspect ratios were advantageous for the design of the foundation and the pylon, whereas it is disadvantageous for the azimuth drive. The same authors studied the efficiency of the drive system to sustain the aerodynamic loads [8]. They used a prototype of a heliostat with rim drives. They showed that, during operation, the heliostat is locked

* e-mail: hmerarda@gmail.com

mechanically and the motors can be faced recurrent switch offs which leads to the power consumption reduction. Wu et al. [9] conducted a study of the effect of gap size between the facets of the heliostats (ranging between 0 and 40 mm) on the overall wind loads. They showed numerically and experimentally that this gap is of negligible effects on the wind loads on heliostat structure. Mammar et al. [10] studied pylon heights effect (68.9, 109.2 and 149.5 mm) on steady/unsteady heliostat wind loads. They showed that the steady and unsteady wind loads increase as the pylon height increases. The effect of heliostat position has been also studied in BLWT experiments by Gong et al. [11]. On the basis of the result analysis, the authors suggest that stow position is the most favorable position to resist wind loads.

Following all the above-mentioned works, it can be assessed that optimal structure design and selection of suitable heliostats parameters, as well as the aspect ratio allow a significant cost reduction in heliostats erection. On the other hand, the selection of suitable part of heliostat, the dimensions and the amount of material used for different parts of the heliostat have significant impacts, regarding the wind loads. Within this frame, the contribution of this work consists in experimental investigation of the impact of the heliostat mirror shapes (square, octagonal and circular) on the wind load. Furthermore, the effect of the flow turbulence intensity and the gap between the lower part of the mirror and the ground are investigated. Using the force balance for a large number of combinations of elevation and yaw angles of the heliostat, the three aerodynamic forces and four moments are measured on reduced scale models of heliostats. The results show that, in smooth flow conditions, the geometry of the mirror has limited effects on the mean force coefficient, while impacting the fluctuating part of the aerodynamic loads. But in turbulence flow conditions, it is necessary to take into account the heliostat0s shape effects on the wind load during the design process of heliostats, especially of elevation drive and mirror support structure. The analysis of the ground effect on the loads on the heliostat when the mirror is set perpendicularly to the wind shows a weak increase of the mean drag force (<5%) and a large increase of the pitching moment (up to 40%). This conclusion is consistent with Mammar et al. [10] findings that an increase in the pylon height produces larger steady and unsteady pressure wind loads.

2 Methodology

This work is based on a measurement campaign carried out at the wind tunnel laboratory of University of Liège. Forces and moments are measured on reduced scale models of heliostats in low, medium and strong turbulence wind conditions in a uniform wind profile. This choice is justified by the fact that boundary layer profiles available in standard codes (such as the Eurocodes [12]) correspond to strong wind features for an isolated structure. In the case of solar field, heliostats located near the perimeter strongly modify the flow impacting heliostats in the middle of a field [13]. As it is the case for PV solar panels located on the roof of low rise buildings [14], a detailed mapping of the flow velocities and corresponding aerodynamic loadings should be performed. Instead, the purpose of this work is to study the effect of the shape of the mirror on the aerodynamic loads. Square, octagonal and circle shapes are tested and compared. The panel area is kept unchanged for the three geometries in order to compare their aerodynamic loadings for the same solar reflection energy. For each geometry, the effect of inclination of the mirror (α and β) and height of the pylon ($\boldsymbol{H}$) is investigated.

2.1 Wind tunnel models

Generally, the reflector surface of the heliostats consists of a set of small mirrors placed with a thin gap between them. It was shown [9] and [15] that the thin gaps between the mirrors have the tendency to slightly increase the global wind loads on the heliostat/PV panel. In this work, all mirrors of model heliostats were replaced by a single panel element: the gap and other details (stiffeners in the back of the mirror) are not represented. This choice is justified by the objective to analyse the effect of the shape of the mirror and to reduce the uncertainty on the reproduction of these small details at reduced scale (local Reynolds effects). Plain square mirrors were also used by Emes et al. [4,16].

The models tested consist in a reduced scale geometry by a factor of 20. This scaling is typical for this type of study and the Reynolds effect was shown limited by Aly and Bitsuamlak [17] in the range 1:5 up to 1:50. The panels are made of aluminum of 2 mm thickness to ensure enough stiffness and hence no static deflection nor vibration, without adding an aerodynamic thickness/bluff-body effects. Square, octagonal and circular heliostat models are shown in Figure 1. The mirror area is equal tag to S = 0.075 m2 and the reference dimensions ($\mathbf{h}$) are equal to 0.274, 0.301 and 0.309 m for the square, octagonal and circular models respectively. Measurements are carried out in the aeronautical test section, characterized by a cross-section of 2×1.5 m2, leading to a maximum blockage ratio of 2.4%, for which no corrections are applied.

The model is supported by a circular pylon (diameter 10 mm) installed on a circular wooden turntable (diameter 0.9 m). The purpose of the turn-table is (i) to be able to change the yaw angle ($\boldsymbol{\beta}$) externally, using the controller of the wind tunnel and (ii) to test the mirror in a spatially uniform wind, that is, limiting the height of the boundary layer impacting the mirror using a short upstream distance. The boundary layer profiles (mean velocity and turbulence intensity) measured by a cobra probe over the turn-table at the location of the model are shown in Figure 2. In this figure, the thick vertical line represents the presence of the mirror at 90° (absent during the measurement of the flow features). It shows that the later lies outside the boundary layer developing on the turn table and all results presented here concern aerodynamic loadings in spatially uniform wind conditions.

2.2 Instrumentation

The mirror of the heliostat is instrumented by a six-components forces/moments balance located just below

Fig. 1. Heliostat models installed in the wind tunnel test section: square (left), octagonal (center), circular (right).

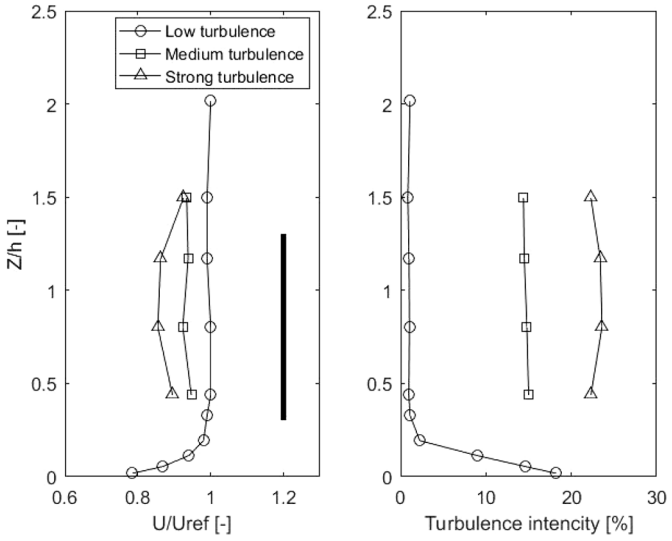

Fig. 2. wind velocity and turbulence intensity of the incoming wind for the low, medium and high turbulent levels.

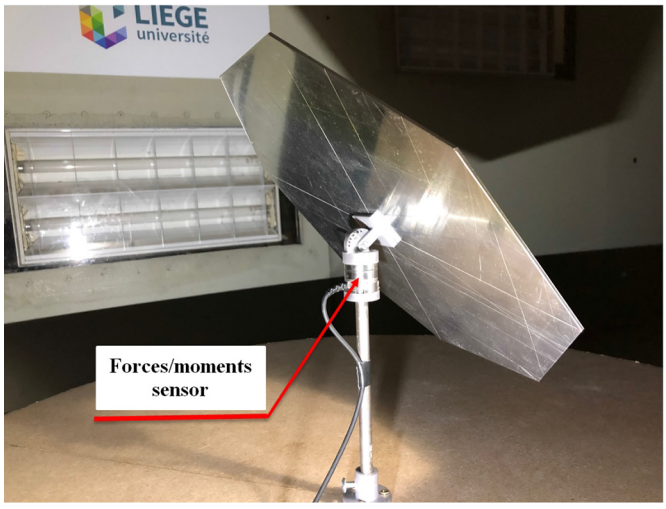

Fig. 3. Force balance mounted on the heliostat.

the surface and close to the center of gravity of the plate (see Fig. 3). A commercially available force balance (ATI NANO 25) is used. A conservative maximum error estimate of 1.56N with 95% confidence level is announced, although the actual precision is expected to be much better because the systematic error is systematically removed by zeroting the sensor before each measurement. The mean aerodynamic forces and moments are computed by averaging measurement signals performed at 50 Hz during 30 s.

The wind speed is classically measured using a Pitot tube located slightly upstream and above the model.

2.3 Aerodynamic Coefficients

The coordinate system proposed by Peterka et al. [18] is retained (see Fig. 4). The force balance is installed between the pylon and the panel elevation link, hence it rotates along the yaw angle but not the elevation angle. All forces presented in this study are expressed in the frame of reference of the wind, leading to the classical denomination of lift and drag forces for $\boldsymbol{F_z}$ and $\boldsymbol{F_x}$ respectively.

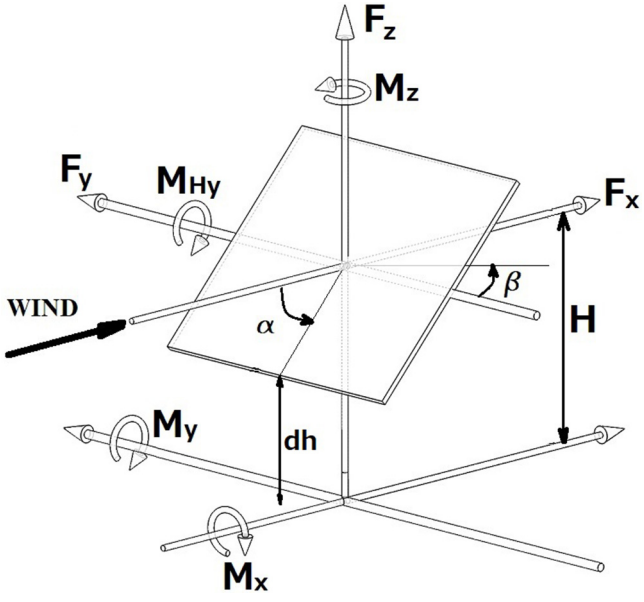

Fig. 4. Coordinate system of heliostat model.

The moments at the basis of the pylon are obtained by equations (1–3).

$$\mathbf{MH_y} = \mathbf{M_y} - \mathbf{F_x}\cdot\mathbf{H} \tag{1}$$

$$\mathbf{M_x} = \mathbf{M_{x,sensor}} + \mathbf{F_y}\cdot\mathbf{\Delta H_{sensor}} \tag{2}$$

$$\mathbf{M_y} = \mathbf{M_{y,sensor}} + \mathbf{F_x}\cdot\mathbf{\Delta H_{sensor}} \tag{3}$$

where $\mathbf{F_y}$ is the side force, $\mathbf{M_{x,sensor}}$ and $\mathbf{M_{y,sensor}}$ are the moments measured by the force balance, $\mathbf{\Delta H}$ sensor is distance between the force balance and the base of the pylon and $\boldsymbol{H}$ is the distance between elevation axis and base of the pylon.

The mean aerodynamic coefficients are calculated according to:

$$\mathbf{CF_i} = \frac{\mathbf{F_i}}{1/2\rho \boldsymbol{V}^2 \boldsymbol{S}} \tag{4}$$

$$\mathbf{CM_i} = \frac{\mathbf{M_i}}{1/2\rho \mathbf{V}^2 \mathbf{SH}} \tag{5}$$

The total wind load coefficient, noted $\boldsymbol{CF}$ is calculated by the vectorial summation of the norms of the coefficients $\boldsymbol{CF_i}$ (i = x, y, z).

3 Results

The measured forces and moments are transformed into non-dimensional aerodynamic coefficients and presented in this section. First, the Reynolds independency is confirmed. On this basis, the aerodynamic coefficients are obtained for different combinations of elevation and yaw angles at a unique wind speed (around 10 m/s for all tests) in low turbulence flow conditions. They are presented sequentially for the three shapes, with comparison with literature results when available. The effect of the shape of heliostat and the vicinity of the ground are investigated through the mean and fluctuating (std) values of selected aerodynamic coefficients. The maximum mean force and moment coefficients are summarized in a table with the corresponding elevation and yaw angles. Finally, the effect of turbulence is investigated through additional tests on the three geometries for a specific configuration of the mirror.

3.1 Reynolds effect

The dependency of the aerodynamic force coefficients is first investigated in the case of the square heliostat for two elevation angles (45° and 90°). The heliostat is kept aligned with the wind, that is, $\boldsymbol{\beta} = \mathbf{0}°$ and the ground distance is set to 20 mm. For that purpose, the wind speed is varied between 6 and 21 m/s, corresponding to a Reynolds range between $\mathbf{1.3 \times 10^5}$ and $\mathbf{4.5 \times 10^5}$. This range is smaller than the full scale Reynolds range (up to $\mathbf{3 \times 10^6}$) but it is commonly used in other wind tunnel analysis of the wind effects on heliostats [17] and more generally in the field wind tunnel testing of bluff-bodies. In this field, the flow separation takes place at the sharp edges of the geometry and the Reynolds effect is limited above $\mathbf{10^5}$.

Figure 5 presents the variation of the mean $\boldsymbol{CF_x}$ and $\boldsymbol{CF_z}$ coefficients with Reynolds number. It is observed that these coefficients are independent of the Reynolds number above the value of $\mathbf{2 \times 10^5}$. Figure 5b includes the results of Bearman [19] for the drag coefficient of a square plate perpendicular to the flow. The difference (13% for the first value and 8% for the leftovers) between the values of the force coefficients of the present work and the ones of Bearman can be attributed to the turbulent flow conditions used by Bearman and the ground effect. Nevertheless, an equivalent independence on the Reynolds number is found in both data sets.

In the rest of the work, all tests have been performed around 10 m/s, which correspond to a Reynolds number of 2×10^5. This value is included in the Reynolds range where the latter has no effect on the resulting aerodynamic coefficients.

3.2 Aerodynamic coefficients

Aerodynamic coefficients are calculated for several combinations of elevation and yaw angles in low turbulence flow conditions. In the first part of this section, the height of the pylon $\mathbf{H}$ is fixed to 202 mm, as sketched in Figure 6. Due to the fixed area of the three heliostats, the resulting gap ($\boldsymbol{dh}$) between the lower part of the panel and the ground is slightly different for the three shapes. It is equal to 65, 51.5 and 47.5 mm for square, octagon and circle respectively.

3.2.1 Square geometry

The lift and drag force coefficients for elevation angles ranging between 0° and 90° are shown in Figure 7 together with the results of Ortiz et al. [20] and Cermak et al. [21] (reproduced from the work of Peterka et al. [18]. The trend of the coefficients versus elevation angle is similar for the three shapes. The slight differences can be attributed to the flow conditions in which the square heliostats were tested: low turbulence (≈1%) and uniform flows are used in the present study and Cermak et al. [21] while boundary layer flows are used by Ortiz et al. [20].

Figure 8 shows the fluctuating component of the force coefficients and compares the present measurements to the results of Ortiz et al. [20]. In both cases, we observe that the fluctuations reach a maximum value when the elevation angle takes values between 30° and 45°, except in the case "close to the wall" reported by Ortiz for the drag component. In the case of the lift component, it can be explained by the strength of the vortices shed at the leading and trailing edges of the heliostat which is maximum when the elevation angle lies in this range.

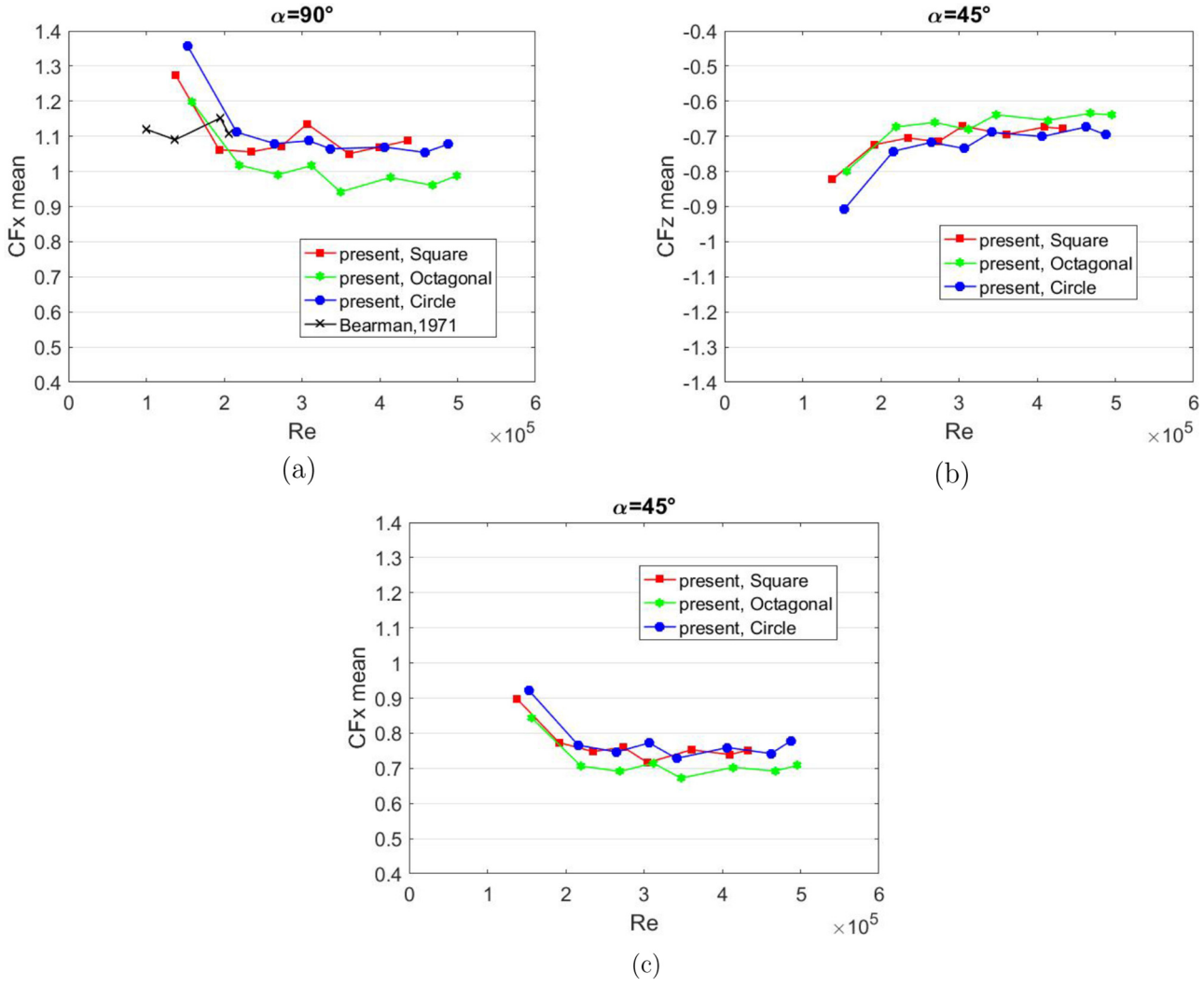

Fig. 5. Reynolds effect on the CF_x and CF_z mean coefficients at $\alpha = 45°$ and 90° for $\beta = 0°$ (square shape in low turbulence flow conditions).

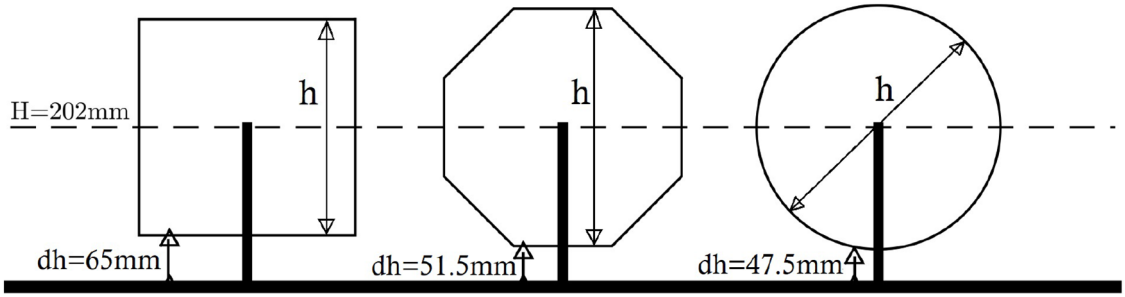

Fig. 6. Sketch of the three shapes.

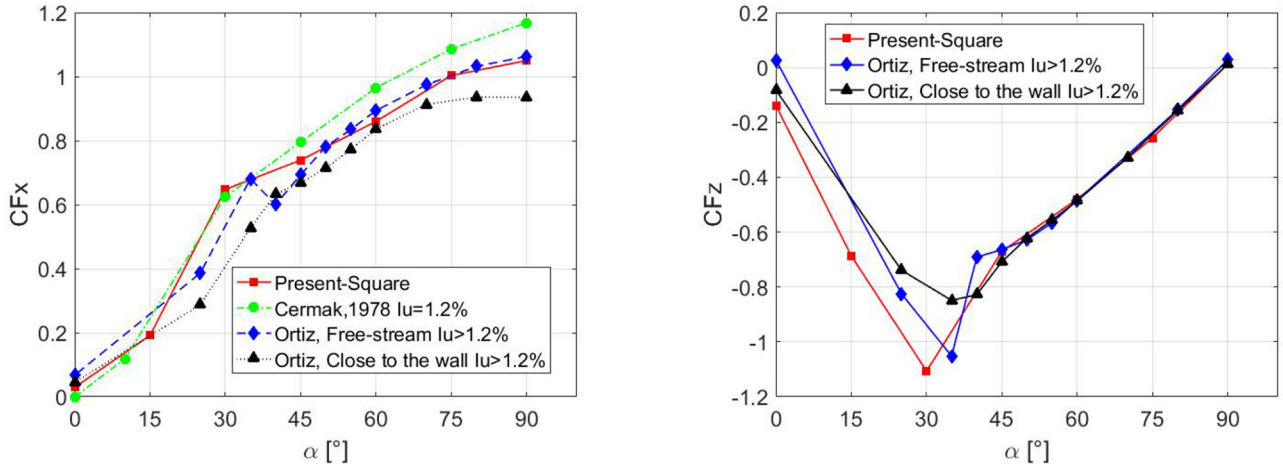

Fig. 7. Mean force coefficient $\boldsymbol{CF_x}$ and $\boldsymbol{CF_z}$, as a function of elevation angle α (square shape in low turbulence flow conditions.

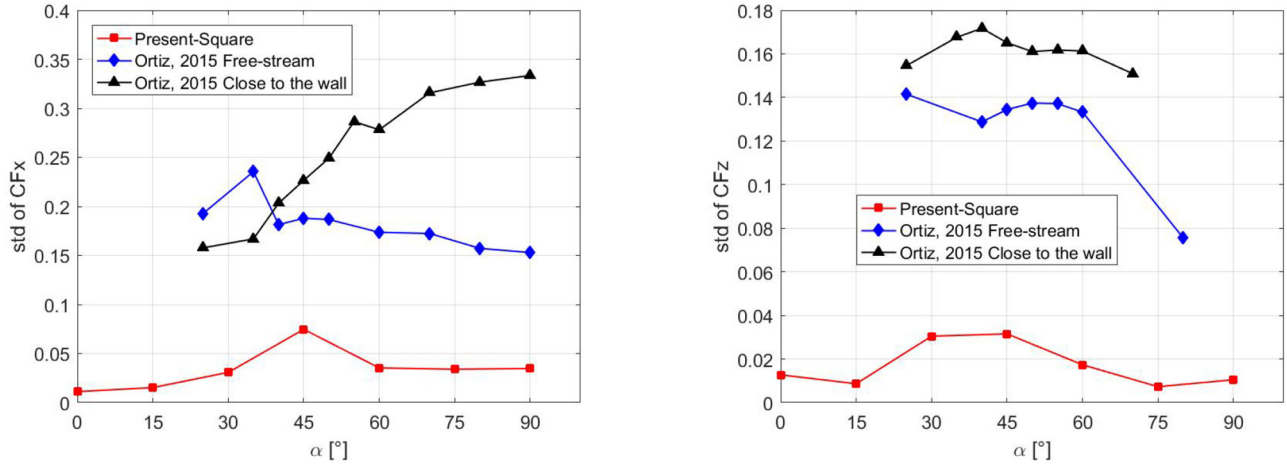

Fig. 8. Fluctuating component (std) of $\boldsymbol{CF_x}$ and $\boldsymbol{CF_z}$, as a function of elevation angle α (square shape in low turbulence flow conditions).

Figure 9 shows the four aerodynamic force coefficients when both the elevation ($\boldsymbol{\alpha}$) and yaw ($\boldsymbol{\beta}$) angles are varied between 0° and 90°, in low turbulence flow conditions.

The following remarks are addressed:

– When the heliostat is aligned with the flow ($\boldsymbol{\beta} = 0°$), the main component of the total aerodynamic force is the lift component for low elevation angles ($\boldsymbol{\alpha} \leq 15°$), that is, before the complete separation of the flow on the surface of the heliostat. Beyond this value, the aerodynamic force consists mainly in a drag component due to pressure differences between both faces of the mirror of the heliostat.

– Some combinations of elevation and yaw angles lead to the same position of the mirror relative to the incoming flow, for example, ($\boldsymbol{\alpha} = 90°$; $\boldsymbol{\beta}$) ≡ ($\boldsymbol{\alpha}$; $\boldsymbol{\beta} = 90°$). The only difference lies in the ground effect. Assuming that separation of the shear layer takes place at the edges of the heliostat, the behavior of these layers is impacted by the presence of the ground. Hence the wake is modified by the presence of the ground and some differences appear in the resulting aerodynamic forces. As an example, the total force coefficient CF is equal to 1.17 for the case ($\boldsymbol{\alpha} = 90°$; $\boldsymbol{\beta} = 45°$) and only 1.02 for its equivalent configuration ($\boldsymbol{\alpha} = 45°$; $\boldsymbol{\beta} = 0°$).

– For the elevation angle $\boldsymbol{\alpha} = 45°$, two yaw angles are tested: $\boldsymbol{\beta} = 0°$ and $\boldsymbol{\beta} = 180°$. It is observed that the drag force is not impacted by the ground effect and presence of the pylon and sensor in front of the heliostat. On the other hand the amplitude of the lift coefficient is reduced in a counter-intuitive manner (see Fig. 10). In this case

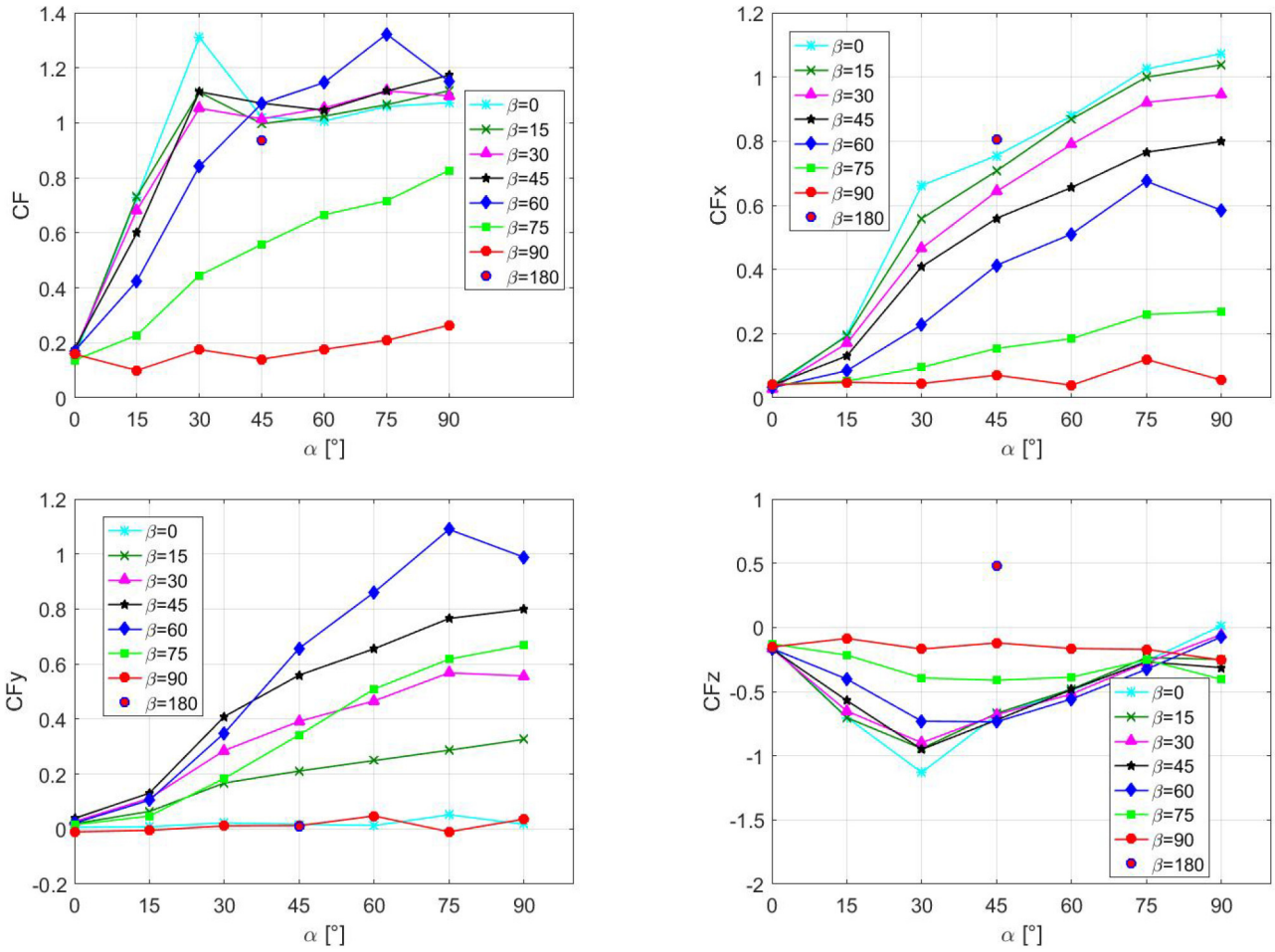

Fig. 9. Mean force coefficients with different orientations (square shape in low turbulence flow conditions).

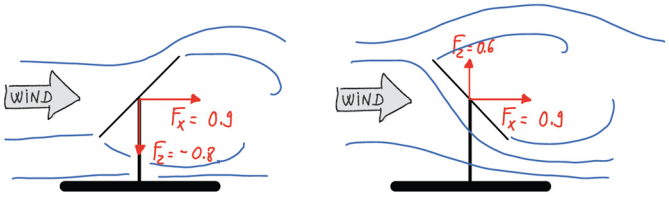

Fig. 10. Sketch of the flow features for $\boldsymbol{\beta} = 0°$ and $\boldsymbol{\beta} = 180°$.

the presence of the sensor and the pylon on the upwind face modifies its pressure field and impacts the vertical force.

Figure 11 shows the moment coefficients. As expected, the largest moments correspond to the base of the pylon ($\mathbf{C_{Mx}}$ and $\mathbf{C_{My}}$), for which the lever arm is large. The aerodynamic moments on the hinge system ($\mathbf{C_{MHy}}$) and on the yaw system ($\mathbf{C_{Mz}}$) are one order of magnitude lower than the ones relative to the base of the pylon.

3.2.2 Octagonal geometry

The octagonal heliostat is tested with the same procedure than the square geometry and still in low turbulence flow conditions. The aerodynamic force and moment coefficients are presented in Figures 12 and 13. These coefficients show the same trends than the square geometry. It is interesting to note that the ground effect is less marked in the case of the octagon despite the fact that this heliostat is slightly closer to the ground than the square one

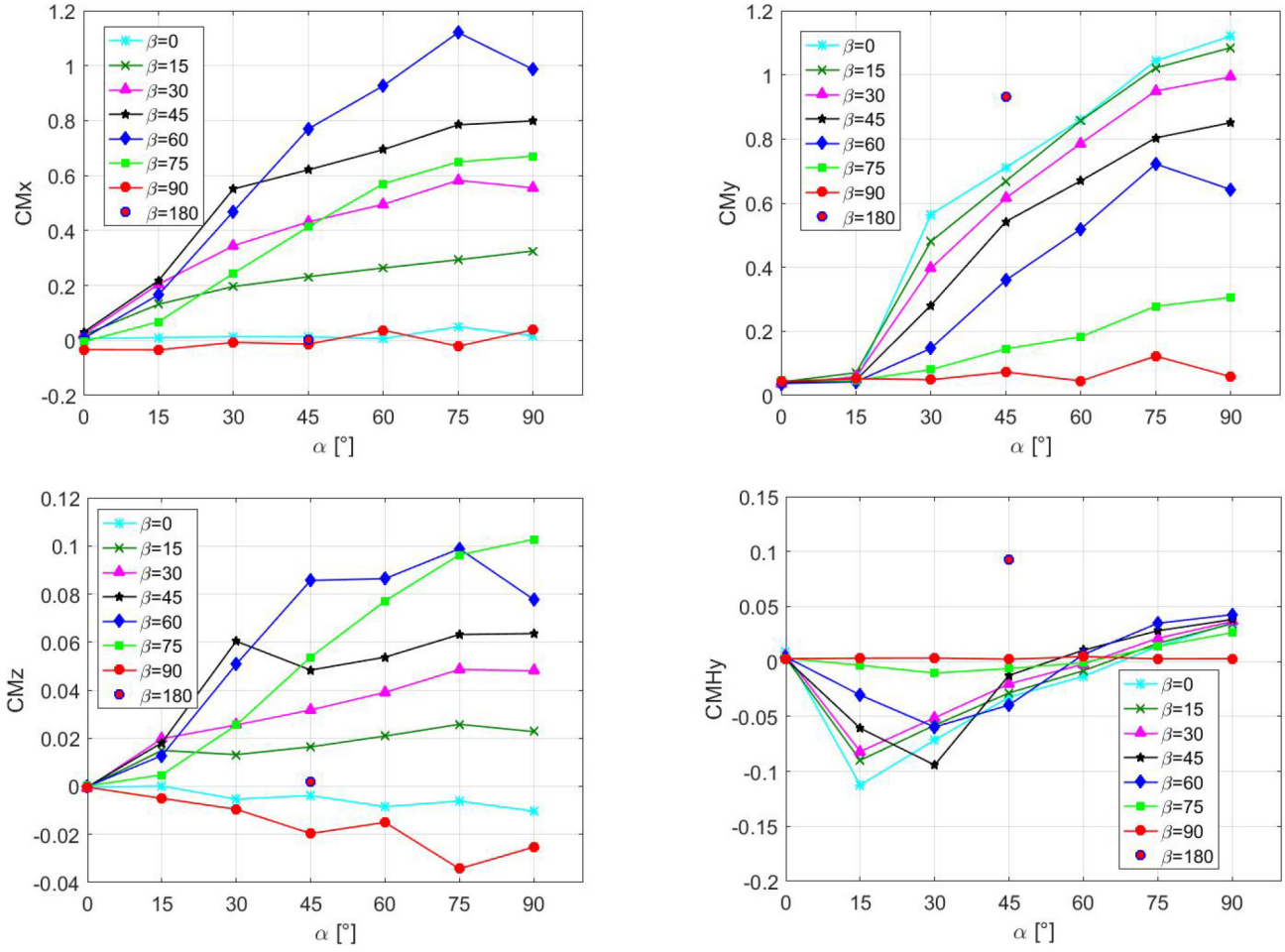

Fig. 11. Mean moment coefficients with different orientations (square shape in low turbulence low conditions).

(see Fig. 6). In this case, the value of the total force coefficient $\boldsymbol{CF}$ is equal to 1.08 for ($\boldsymbol{\alpha} = 90°$; $\boldsymbol{\beta} = 45°$) and 1.01 for its equivalent ($\boldsymbol{\alpha} = 45°$; $\boldsymbol{\beta} = 0°$). The maximum value of the total mean force coefficient CF for octagonal shape is equal to 1.231 for ($\boldsymbol{\alpha} = 30°$; $\boldsymbol{\beta} = 15°$) while is equal to 1.323 and 1.543 for square for ($\boldsymbol{\alpha} = 75°$; $\boldsymbol{\beta} = 60°$) and circle for ($\boldsymbol{\alpha} = 45°$; $\boldsymbol{\beta} = 45°$) respectively. Hence its relative difference drops from 7% with square shape and 20% with circular shape. One difference that can also be highlighted is that the maximum values of the mean lift coefficients $\boldsymbol{C_{Fz}}$ occur for $\boldsymbol{\alpha} = 15°$ for the octagon compared to $\boldsymbol{\alpha} = 30°$ for the square.

3.2.3 Circular geometry

The same trends than the two previous geometries are observed for the aerodynamic load coefficients of the circular heliostat in Figures 14 and 15. The maximum value of the total mean force coefficient $\boldsymbol{C_F}$ for circular shape is equal to 1.543 for ($\boldsymbol{\alpha} = 45°$; $\boldsymbol{\beta} = 45°$). Hence its relative difference of 14% with square shape and of 20% with octagonal shape. An interesting difference is also the maximum value of $\boldsymbol{C_{Fz}}$ for the circular shape for ($\boldsymbol{\alpha} = 45°$; $\boldsymbol{\beta} = 45°$) greater than its value for the square and octagon shapes at same angles.

3.3 Shape effect

The total aerodynamic force coefficients of octagonal and circular heliostats are compared to the ones of the square geometry for all combinations of elevation and yaw angles. This analysis is carried out in low turbulence flow conditions.

Figure 16 shows the mean values of $\mathbf{C_F}$ and the corresponding relative differences for the three shapes. Quantitatively, the relative difference in comparison with the square geometry is generally lower than 50%, except the configurations ($\boldsymbol{\alpha} = 15°$; $\boldsymbol{\beta}$) for the octagonal geometry where it reaches 200%. The large differences (≥50%) between octagon and square shape for ($\boldsymbol{\alpha} = 15°$; $\boldsymbol{\beta}$) is can be

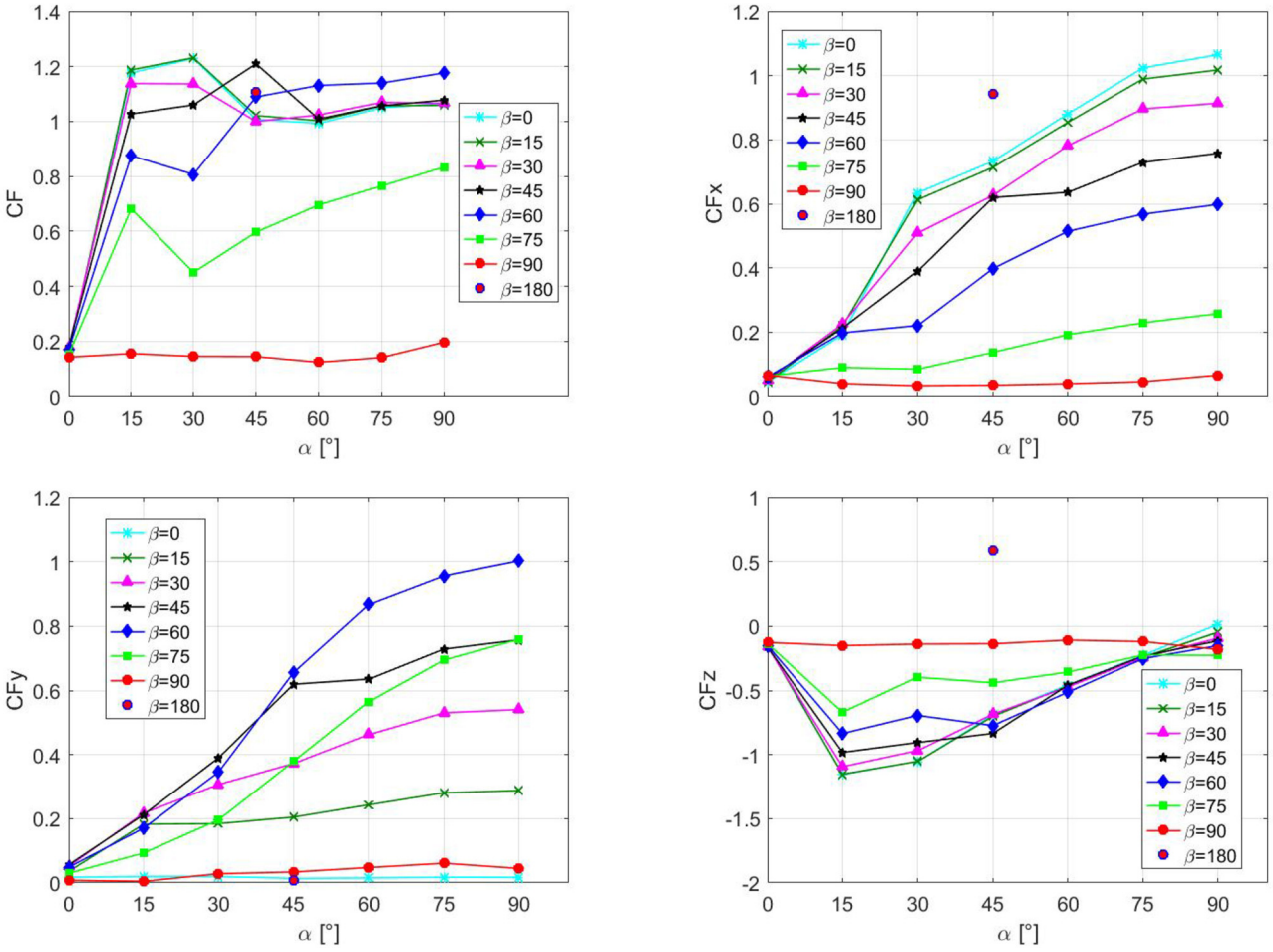

Fig. 12. Mean force coefficients with different orientations (octagonal shape in low turbulence flow conditions).

because of the multiple flat edges for the octagonal shape. It is concluded that the octagonal geometry has an important effect on mean total aerodynamic force for ($\boldsymbol{\alpha} = 15°$).

Things are different concerning the fluctuating component of the total force coefficient (Fig. 17). Many combinations differ by more than $\pm 50\%$ in comparison with the square heliostat. This observation can be justified by the different behavior of the shear layers in the wake of the heliostat. In absence of turbulence in the incoming wind, the unsteadiness of the shear layer is the sole responsible for these fluctuations of the force coefficients. The aerodynamic signature of the heliostats is different because of the geometric differences of edges: single flat edges for the square, multiple flat edges for the octagon and continuous rounded edges for the circle.

3.4 Maximum loadings

The maximum mean values of the eight aerodynamic coefficients in low turbulence flow conditions are presented in Table 1. For each maximum mean value, the corresponding configuration (elevation and yaw angles) are reported. These values can be used to obtain the envelope of aerodynamic forces and moments to be applied at the design stage of the heliostat and its supporting system. The effect of turbulence of the incoming wind can be included in the envelope through a normative approach in order to obtain the peak velocity pressure (depending on the wind characteristics of the site), to be multiplied by the aerodynamic coefficients of Table 1. The largest value of mean total force is experienced by the circle shape with value 1.54 against 1.32 and 1.23 for square and octagon respectively. However, on the mechanical point of view only, the circular shape is the most favorable for the dimensioning of the foundation, the pylon, the elevation drive and azimuth drive. Indeed, the circular shape has the lower values of the aerodynamic moment coefficients.

3.5 Height effect

The effect of the gap (***dh***) between the lower part of the mirror and the ground is investigated for the heliostat set

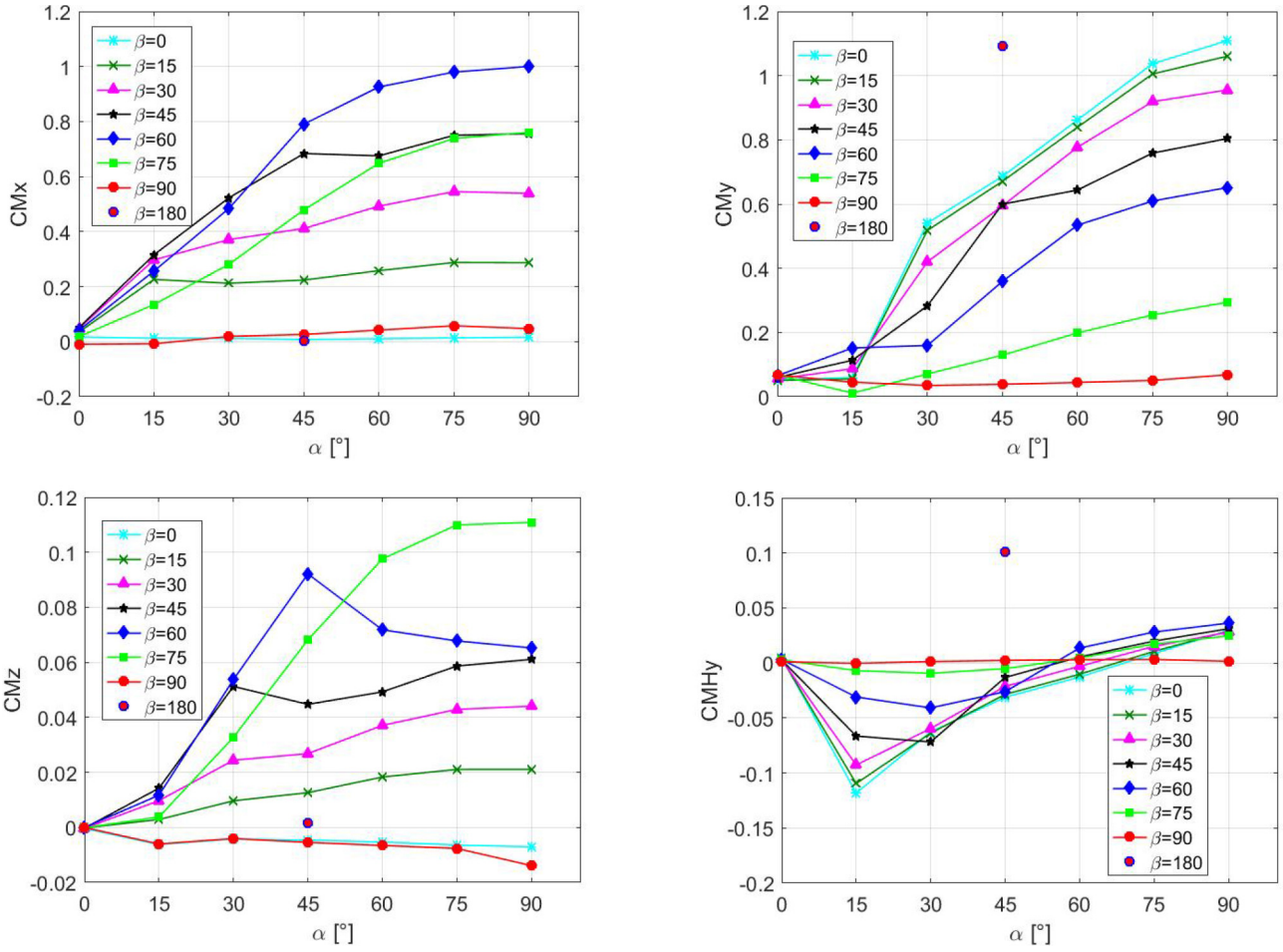

Fig. 13. Mean moment coefficients with different orientations (octagonal shape in low turbulence flow conditions).

Table 1. Maximum mean aerodynamic coefficients of three geometries (low turbulence flow conditions).

Loads	Square			Octagon			Circle		
	α [°]	β [°]	Value	α [°]	β [°]	Value	α [°]	β [°]	Value
$\mathbf{C_F}$	75	60	1.32	30 (30)	0 (15)	1.23	45	45	1.54
$\mathbf{C_{Fx}}$	90	0	1.07	90	0	1.06	90	0	1.04
$\mathbf{C_{Fy}}$	75	60	1.09	90	60	1.00	90	60	1.07
$\mathbf{C_{Fz}}$	30	0	−1.13	15 (15)	0 (15)	−1.15	45	45	−1.21
$\mathbf{C_{Mx}}$	75	60	1.12	90	60	1.00	90	60	1.07
$\mathbf{C_{My}}$	90	0	1.12	90	0	1.11	90	0	1.09
$\mathbf{C_{Mz}}$	90	75	0.10	90	75	0.11	75	75	0.10
$\mathbf{C_{MHy}}$	15	0	−0.11	15	0	−0.12	15	0	−0.10

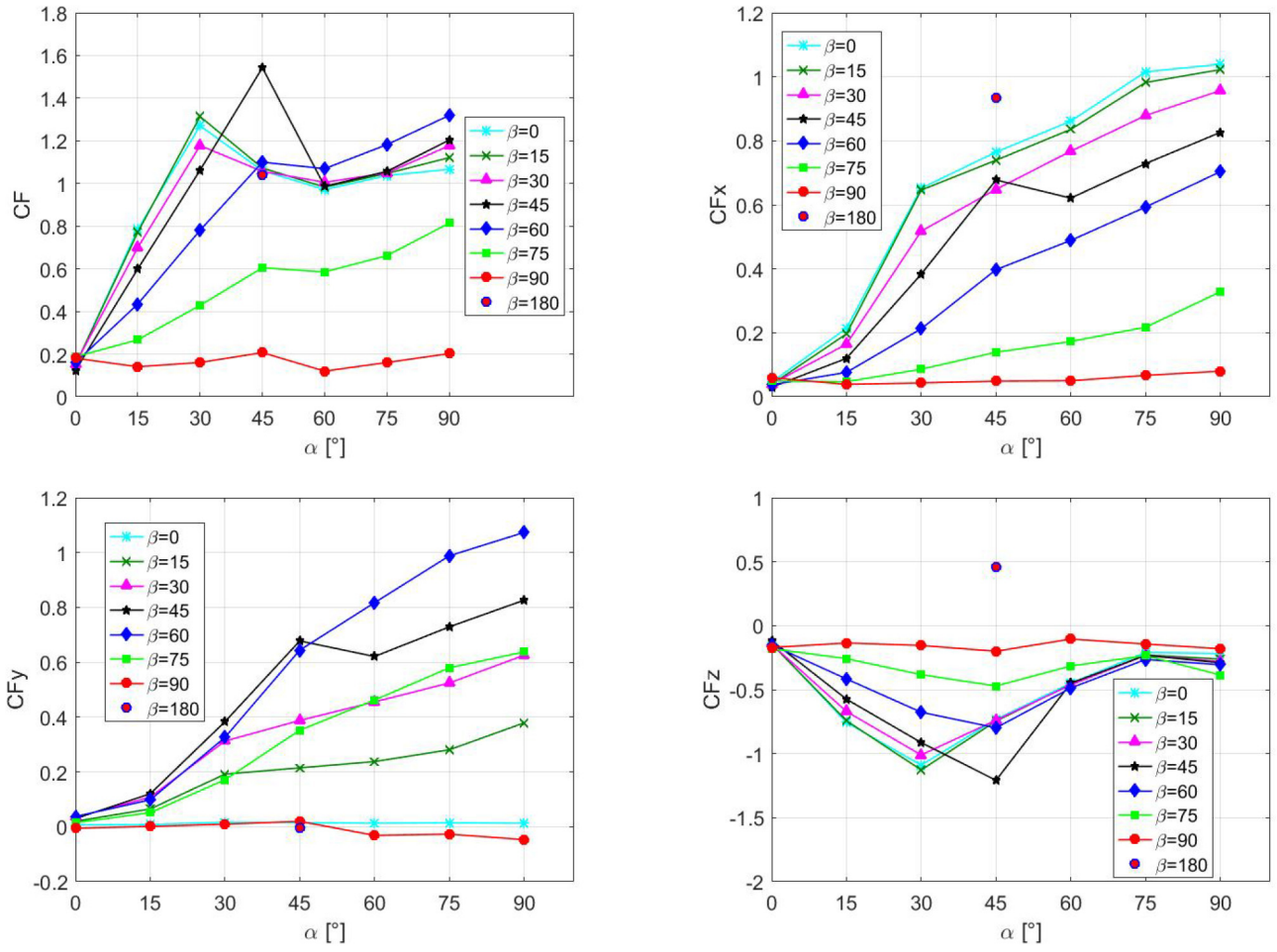

Fig. 14. Mean force coefficients with different orientations (circular shape in low turbulence flow conditions).

perpendicular to the flow. Low turbulent flow conditions are considered here. Figure 18 shows the aerodynamic coefficients as a function of the non-dimensional gap $\boldsymbol{dh/h}$. For this configuration ($\boldsymbol{\alpha} = 90°$, $\boldsymbol{\beta} = 0°$), it is observed that increasing the gap leads to a slight increase of the aerodynamic coefficients. This effect is very low (<5%) for the drag force and more important hinge moment (increase up to 60%).

3.6 Turbulence effect

The effect of the turbulence is investigated in the configuration of elevation angle $\boldsymbol{\alpha} = \mathbf{45°}$ and azimuth angle $\boldsymbol{\beta} = \mathbf{0°}$. Three wind flow conditions are compared: (i) low turbulence presented above ($\boldsymbol{Iu} = \mathbf{1\%}$), (ii) medium turbulence ($\boldsymbol{Iu} = \mathbf{15\%}$) and strong turbulence ($\boldsymbol{Iu} = \mathbf{25\%}$). The turbulence intensity of the flow is adjusted in the wind tunnel test section by the adjunction of passive grids upstream the model. Details about the turbulence generation can be found in Vita et al. [22]. The corresponding mean velocity and turbulence intensity profiles are shown in Figure 2. The corresponding integral length scales, calculated from the first zero-crossing of the autocorrelation function is equal to ≈3.4 cm, that is, of the order to 10% of the characteristic dimension of the mirrors.

Figures 19 and 20 show the mean and peak aerodynamic coefficients as a function of the turbulence intensity. It is observed that the absolute value of the mean and peak aerodynamic coefficients increase monotonically with the turbulence intensity of the incoming flow. The maximum increase is +30% for the mean coefficients, while it reaches +60% for the peak component. This effect on the mean drag force ($\mathbf{CF_x}$ in Fig. 19) is in accordance with the observations of Cermak et al. [21] and Peterka et al. [18] on a square mirror. The aerodynamic load coefficients measured in this work are smaller than the ones reported by Emes et al. [16] and Peterka et al. [18] (for a square mirror). This difference can be attributed to the characteristics of the incoming turbulent winds for the different

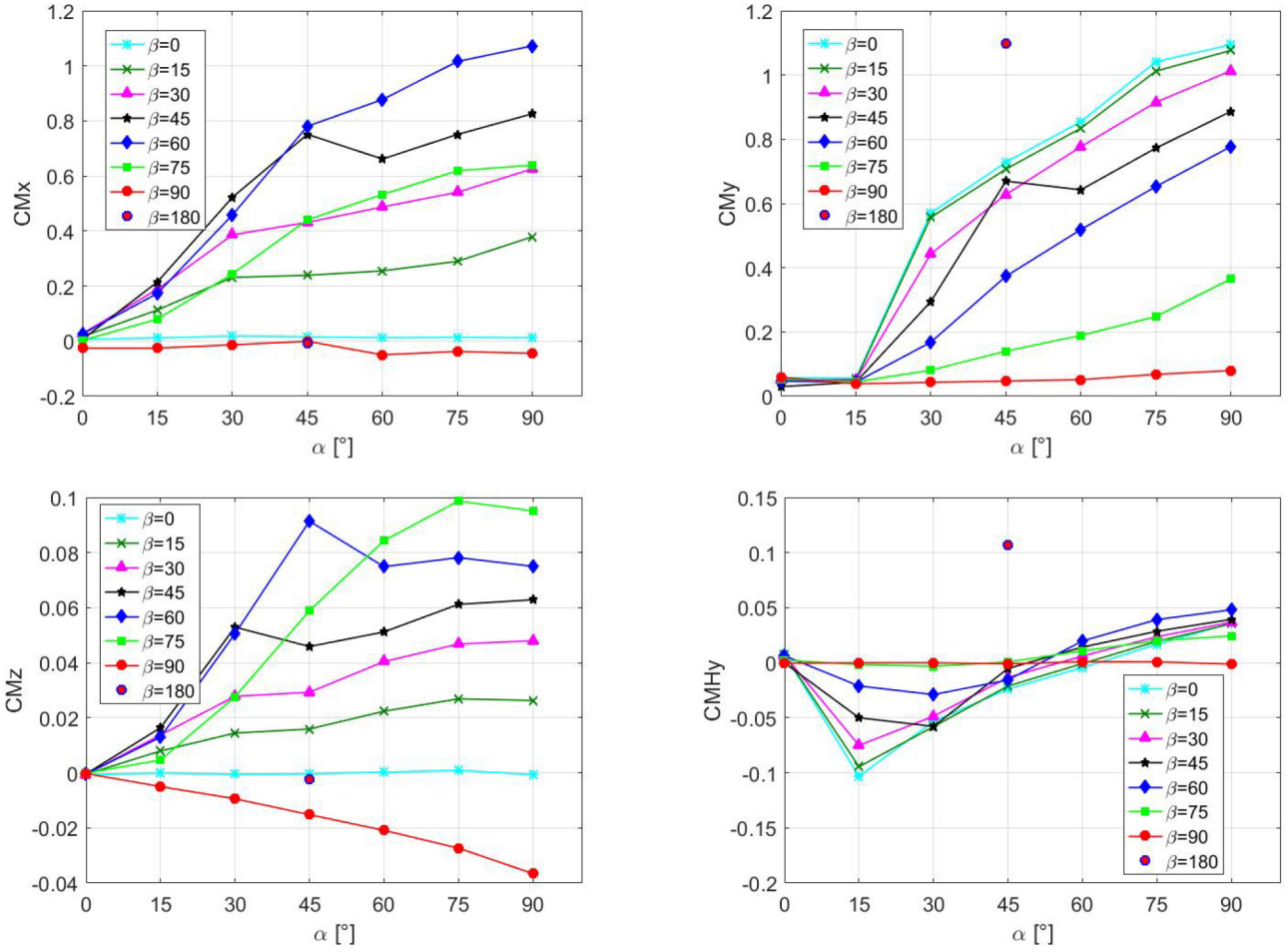

Fig. 15. Mean moment coefficients with different orientations (circular shape in low turbulence flow conditions).

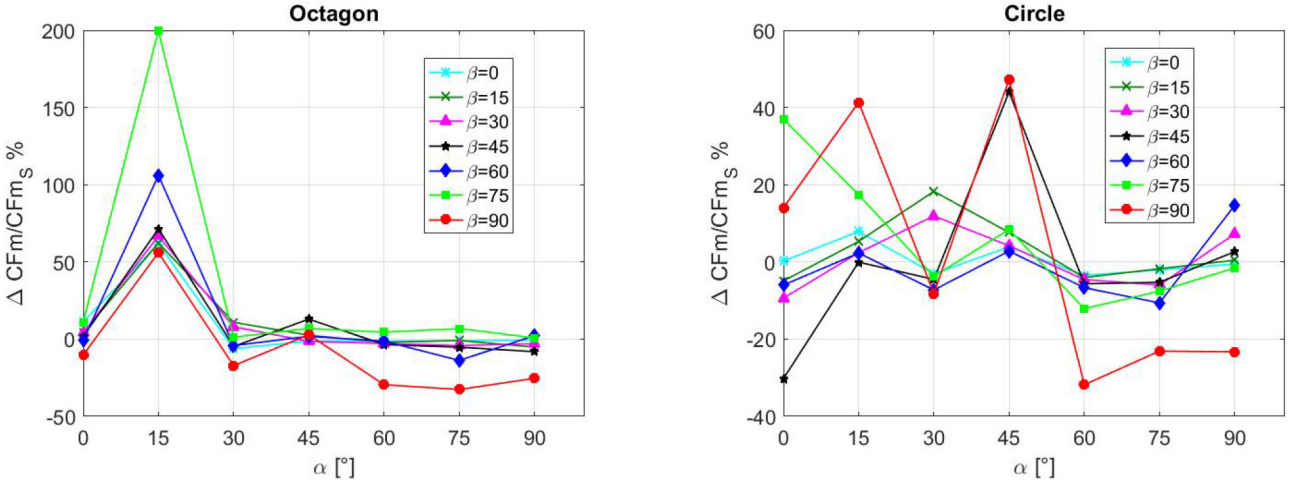

Fig. 16. Relative differences of mean force coefficients for the different shapes [%] in low turbulence flow conditions.

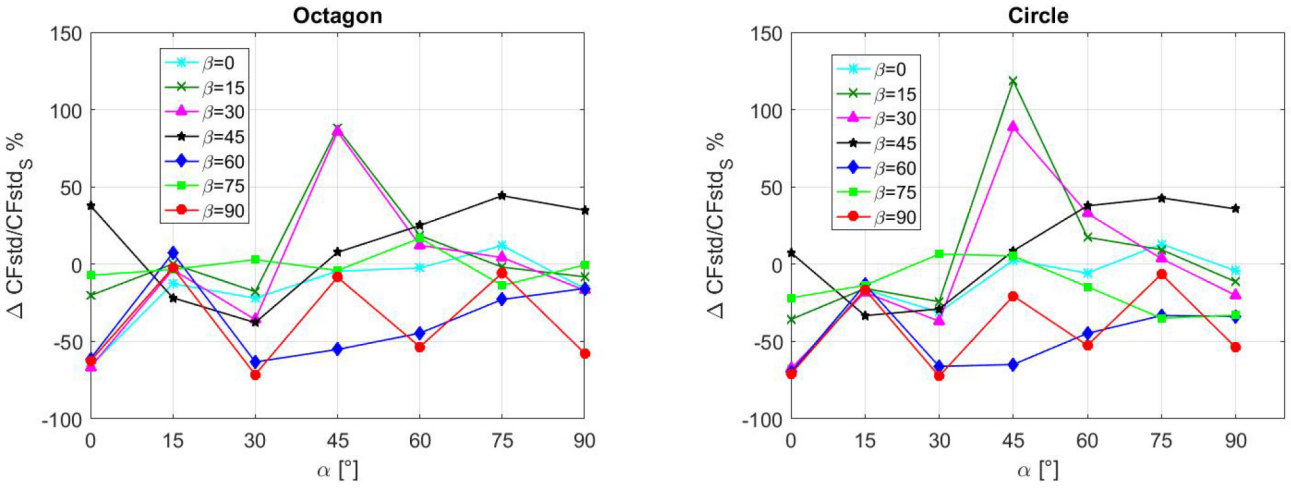

Fig. 17. Relative differences fluctuating (std) of force coefficients for the different shapes [%] in low turbulence flow conditions.

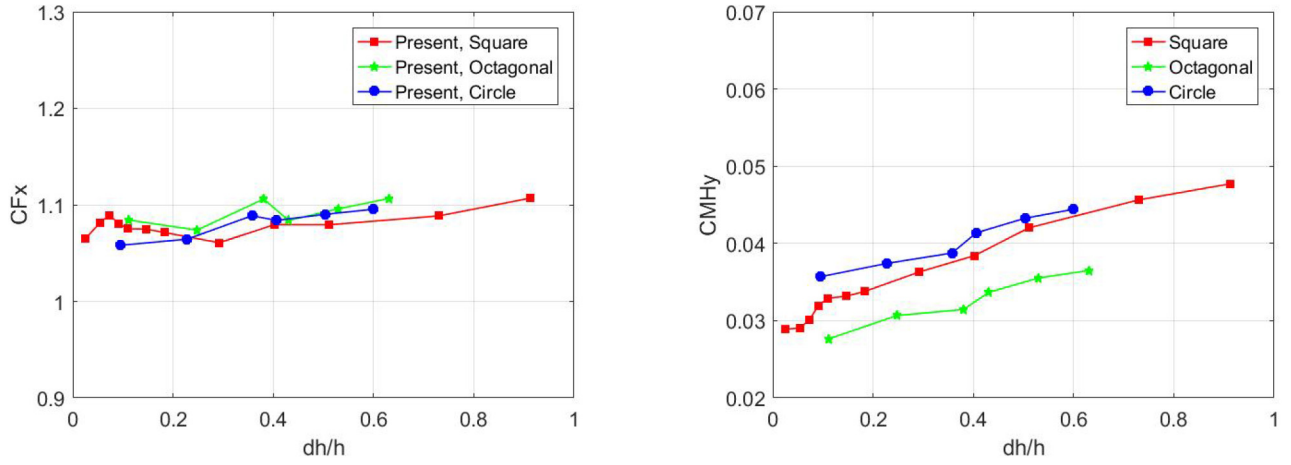

Fig. 18. Height effect on the mean force and moment coefficients, $\alpha = 90°$ and $\beta = 0°$ (low turbulence flow conditions).

studies. In particular the ratio of the longitudinal integral length scale to the reference dimension of the mirror ($\mathbf{L_{ux}} = \mathbf{h}$) of literature works are of the order to ≈2.5, while it is only equal to ≈0.1 in the present study. This difference in $\mathbf{L_{ux}}$ means that the turbulent eddies of the flow impacts locally the mirror in the present study while it encloses totally the mirrors in the works of Emes et al. [16] and Peterka et al. [18].

The turbulence effect on the mean and peak aerodynamic coefficients is similar for the three shapes. Nevertheless, the aerodynamic loading is less severe for the circular geometry, especially for the mean hinge moment (mean $\mathbf{C_{MHy}}$ in Fig. 19) and the peak hinge and lift coefficients (peaks $\mathbf{C_{MHy}}$ and $\mathbf{C_{Fz}}$ in Fig. 20). For highest level of turbulence, the reductions of the mean and peak aerodynamic moment reaches −15 and −3% for the circular mirror in comparison with the square geometry. The reduction of the peak lift coefficient is equal to −5%. The opposite observation is made for the octagonal shape: increases of 10% (for mean $\boldsymbol{C_{MHy}}$), 15% (for peak $\boldsymbol{C_{MHy}}$) and 2% (for peak $\boldsymbol{C_{Fz}}$) are reported in comparison with the square geometry.

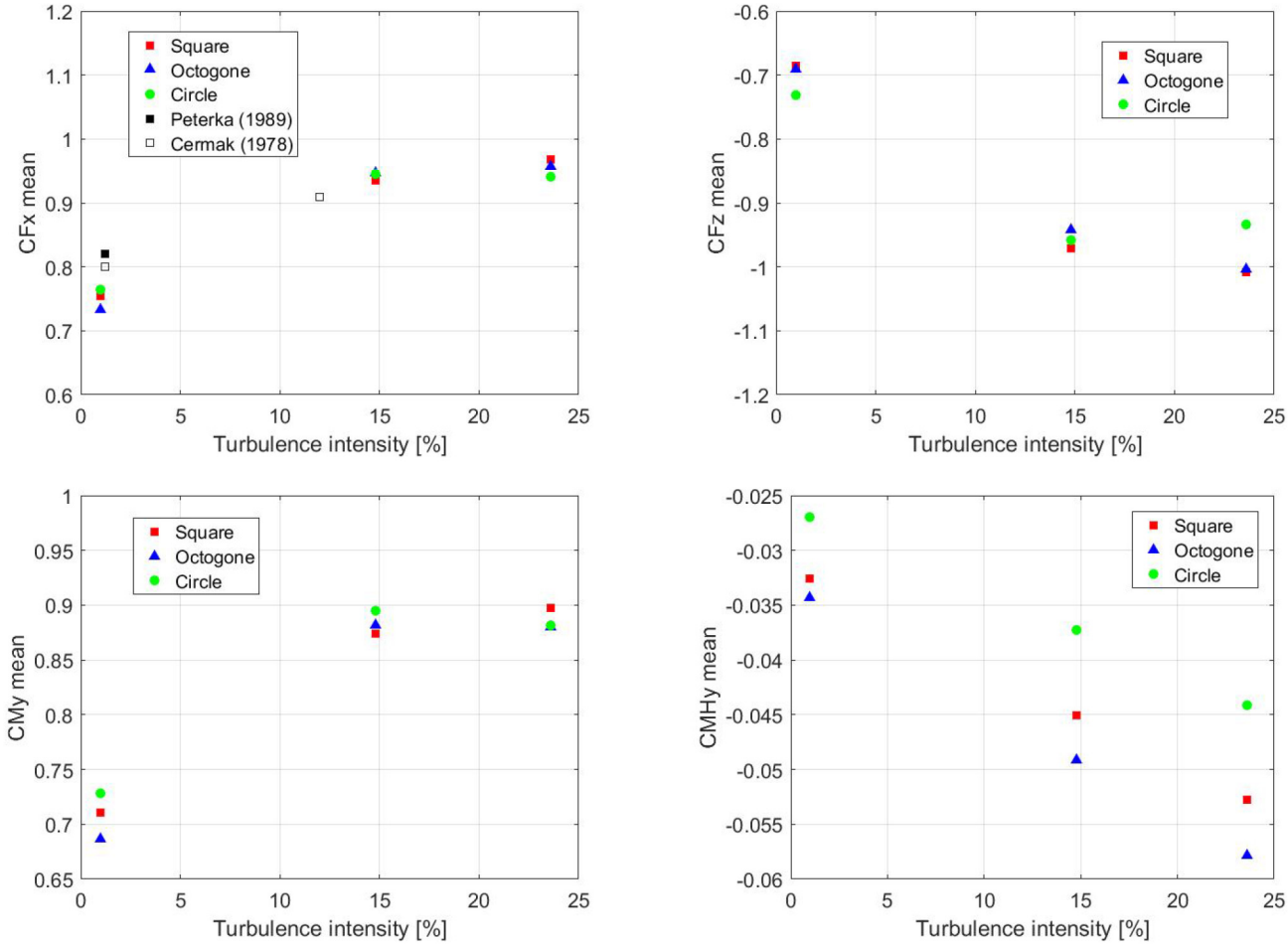

Fig. 19. Turbulence effect on the mean force and moment coefficients ($\alpha = 45°$, $\beta = 0°$).

4 Conclusion

The effect of the shape of the mirror of heliostats on the aerodynamic loading is investigated through wind tunnel testing. Forces and moments measurements are carried out on three geometries: square, circular and octagonal. The heliostat is tested in stand alone configuration in spatially uniforms, smooth and turbulent flow conditions. These conditions are not representative of the real position of a heliostat within a solar field (made of hundreds of heliostats). Nevertheless the objective here is to quantify the effect of the shape and height on the aerodynamic coefficients. The area of the three mirrors is kept constant for sake of comparison of the potential solar energy to harvest.

The following conclusions are drawn: in low turbulence flow conditions ($\boldsymbol{Iu} = \mathbf{1\%}$), the shape of the mirror does not impact the mean aerodynamic coefficients; while the fluctuating components of the aerodynamic forces are modified. In turbulent flow conditions ($\boldsymbol{I_u} > 15\%$), the circular mirror geometry is advantageous in the specific case of aligned wind with an inclination of $\boldsymbol{\alpha} = 45°$. The effect of height in the configuration where the wind is perpendicular to the mirror is limited to 5% for the drag force but it can increase by 60% for the hinge moment.

On a purely aerodynamic point of view the circular geometry is advantageous to reduce the mean and peak wind loads on the heliostat. This assessment is limited to the generic configuration of a heliostat inclined of $\boldsymbol{\alpha} = 45°$ and $\boldsymbol{\beta} = 0°$ in a uniform wind. Hence, the circular mirror shape is advantageous for the aerodynamic design of the elevation drive and mirror/panel support structure of heliostats and solar trackers.

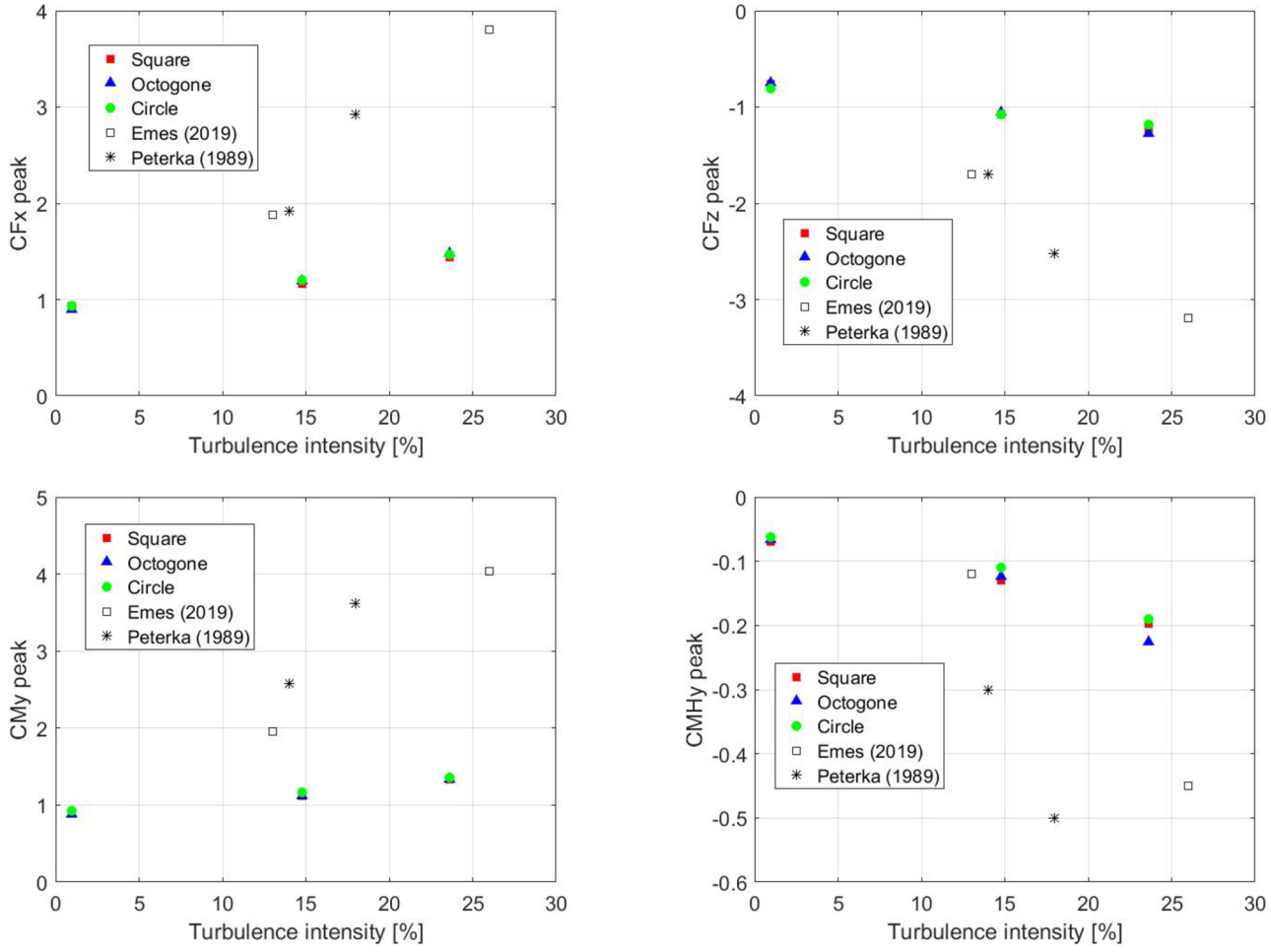

Fig. 20. Turbulence effect on the peak force and moment coefficients ($\alpha = 45°$, $\beta = 0°$).

Notations

h	Reference dimension of the mirror [m]
dh	Height of the gap between the lower part of the mirror and the ground [m]
H	Height of the pylon [m]
S	Reference surface [m2]
V	Wind speed [m/s]
I_u	Turbulence intensity [%]
L_{ux}	Longitudinal integral length scale [m]
C_{Fi}	Aerodynamic force coefficient in the X,Y, Z directions [–]
C_{Mi}	Aerodynamic moment coefficient in the X,Y, Z directions [–]
C_{MHy}	Aerodynamic moment coefficient in the Y direction at the location of the hinge system [–]
α	Elevation angle of mirror plane, 0° when horizontal [°]
β	Wind direction, 0° when perpendicular to elevation axis [°]
ρ	Density of air [kg/m3]
x	Coordinate, horizontal, perpendicular to elevation axis, at pylon base
y	Coordinate, horizontal, along elevation axis, at pylon base
z	Coordinate, vertical upwards (azimuth axis)

References

[1] A. Pfahl, J. Coventry, M. Röger, F. Wolfertstetter, J.F. V'asquez-Arango, F. Gross, M. Arjomandi, P. Schwarzbözl, M. Geiger, P. Liedke, Progress in heliostat development, Solar Energy **152**, 3–37 (2017)

[2] G.J. Kolb, S.A. Jones, M.W. Donnelly, D. Gorman, R. Thomas, R. Davenport, R. Lumia, Heliostat cost reduction study. Sandia National Laboratories, Albuquerque, NM, Report No. **SAND2007-3293**, 103 (2007)

[3] M.J. Emes, M. Arjomandi, G.J. Nathan, Effect of heliostat design wind speed on the levelised cost of electricity from concentrating solar thermal power tower plants, Solar Energy **115**, 441–451 (2015)
[4] M.J. Emes, M. Arjomandi, F. Ghanadi, R.M. Kelso, Effect of turbulence characteristics in the atmospheric surface layer on the peak wind loads on heliostats in stow position. Solar Energy **157**, 284–297 (2017)
[5] J.A. Peterka, B. Bienkiewicz, B.N. Hosoya, J.E. Cermak, Heliostat mean wind load reduction, Energy **314**, 261–267 (1987)
[6] A. Pfahl, H. Uhlemann, Wind loads on heliostats and photovoltaic trackers at various reynolds numbers, Journal of Wind Engineering and Industrial Aerodynamics **99**, 964–968 (2011)
[7] A. Pfahl, M. Buselmeier, M. Zaschke, Wind loads on heliostats and photovoltaic trackers of various aspect ratios, Solar Energy **85**, 2185–2201 (2011)
[8] A. Pfahl, M. Randt, C. Holze, S. Unterschütz, Autonomous light-weight heliostat with rim drives, Solar Energy **92**, 230–240 (2013)
[9] Z. Wu, B. Gong, Z. Wang, Z. Li, C. Zang, An experimental and numerical study of the gap effect on wind load on heliostat, Renewable Energy **35**(4), 797–806 (2010)
[10] M. Mammar, S. Djouimaa, U. Gartner, A. Hamidat, Wind loads on heliostats of various column heights: an experimental study. Energy **143**, 867–880 (2018)
[11] B. Gong, Z. Li, Z. Wang, Y. Wang, Wind-induced dynamic response of heliostat, Renewable Energy **38**, 206–213 (2012)
[12] NBN EN 1991-1-4 ABN. Eurocode 1: Actions on structures-Part 1-4: General actions-Wind actions, National Annex (2010)
[13] NASA Ames, Heliostat flow visualization experiments. Fluid Mechanic Laboratory (2011)
[14] C. Chia-Ren, T. Sheng-Jue, Aerodynamic loading of solar trackers on flat-roofed buildings, Journal of Wind Engineering and Industrial Aerodynamics **175**, 202–212 (2018)
[15] A. Ayodeji, H. Horia, S. Kamran, Experimental investigation of wind effects on a standalone photovoltaic (PV) module, Renewable Energy **78**, 657–665 (2015)
[16] M.J. Emes, A. Jafari, F. Ghanadi, M. Arjomandi, Hinge and overturning moments due to unsteady heliostat pressure distributions in a turbulent atmospheric boundary layer, Solar Energy **193**, 604–617 (2019)
[17] A.M. Aly, G. Bitsuamlak, Aerodynamics of ground-mounted solar panels: test model scale effects, Journal of Wind Engineering and Industrial Aerodynamics **123**, 250–260 (2013)
[18] J.A. Peterka, Z. Tan, J.E. Cermak, B. Bienkiewicz, Mean and peak wind loads on heliostats, Journal of Solar Energy Engineering **111**, 158–164 (1989)
[19] P.W. Bearman, An investigation of the forces on flat plates normal to a turbulent flow, Journal of Fluid Mechanics **46**, 177–198 (1971)
[20] X. Ortiz, D. Rival, D. Wood, Forces and moments on flat plates of small aspect ratio with application to PV wind loads and small wind turbine blades. Energies **8**, 2438–2453 (2015)
[21] J.E. Cermak, J.A. Peterka, A. Kareem, Heliostat field array wind tunnel test, Report CER78-79JEC-JAP-AK2, Fluid Mechanics and Wind Engineering Program, Colorado State University (1978)
[22] G. Vita, H. Hemida, T. Andrianne, C. Baniotopoulos, Generating atmospheric turbulence using passive grids in an expansion test section of a wind tunnel, Journal of Wind Engineering and Industrial Aerodynamics **178**, 91–104 (2018)

Cite this article as: H. Merarda, M. Aksas, T. Andrianne, Shape Effects on Aerodynamic Loading of Heliostats, Mechanics & Industry **21**, 614 (2020)